

# Magnetic phases in the $S=1$ Shastry-Sutherland model with uniaxial anisotropy

Lei Su, Keola Wierschem and Pinaki Sengupta

*School of Physical and Mathematical Sciences, Nanyang Technological University, 21 Nanyang Link, Singapore 637371*

(Dated: September 1, 2018)

We explore the field induced magnetic phases of an  $S = 1$   $XXZ$  model with single-ion anisotropy and large Ising-like anisotropy on a Shastry Sutherland lattice over a wide range of Hamiltonian parameters and applied magnetic field. The multitude of ground state phases are characterized in detail in terms of their thermodynamic properties and the underlying classical (Ising limit) spin arrangements for the plateau phases are identified by calculating the static structure factors. The enlarged local Hilbert space of the  $S = 1$  spins results in several new ground state phases that are not realized for  $S = 1/2$  spins. These include the quantum paramagnetic state that is ubiquitous to  $S = 1$  spins with single ion anisotropy, two different spin supersolid phases (with distinct longitudinal ordering) and a magnetization plateau that arises as a direct descendant of the  $1/3$  plateau due to quantum fluctuations that are not possible for  $S = 1/2$  spins. We predict the same mechanism will lead to plateaus at smaller fractions of  $1/3$  for higher spins. The full momentum dependence of the longitudinal and transverse components of the static structure factor is calculated in the spin supersolid phase to demonstrate the simultaneous existence of diagonal and off-diagonal long-range order as well as the different longitudinal orderings.

PACS numbers: 75.30.Kz, 02.70.Ss

## INTRODUCTION

The Shastry-Sutherland model (SSM) provides a paradigm to investigate the emergence of novel quantum phases from the interplay between strong interactions, enhanced quantum fluctuations due to reduced dimensionality, geometric frustration and external magnetic fields [1]. The model exhibits a rich variety of ground state phases with varying Hamiltonian parameters. The discovery of  $\text{SrCu}_2(\text{BO}_3)_2$  and the observation of magnetization plateaus in an external field garnered widespread interest and led to extensive investigation of the properties of the material and the underlying SSM using both experimental and theoretical approaches [2–7]. Recently, several additional spin systems have been shown to possess the same underlying magnetic lattice, viz., the Shastry-Sutherland lattice. These include a complete family of rare-earth tetraborides ( $\text{RB}_4$ ,  $\text{R} = \text{Tm}, \text{Er}, \text{Tb}, \text{Ho}, \text{Dy}$ ) [8–10] and the intermetallic  $\text{Yb}_2\text{Pt}_2\text{Pb}$  [11, 12]. Preliminary investigations into the magnetic properties of  $\text{RB}_4$  compounds have revealed that the canonical SSM needs to be supplemented by additional longer range interactions to correctly account for the behavior of these compounds [13, 14].

So far, the theoretical investigations of the SSM have almost exclusively focused on  $S = 1/2$  moments. Although the  $\text{RB}_4$  compounds carry  $S > 1/2$  moments, the local Hilbert space of the localized f-moments in many of these compounds is usually split by a strong single-ion anisotropy into doublets and the low-energy physics is adequately described by the lowest doublet in terms of an effective  $S = 1/2$   $XXZ$  model with strong Ising-like exchange anisotropy. The SSM with  $S > 1/2$  moments has remained largely unexplored, although the importance of such extensions were realized in the original work of

Shastry and Sutherland. The enlarged Hilbert space of larger spins is expected to allow for phases that are not found in the  $S = 1/2$  variant of the model. In this work, we have addressed this by studying the  $S = 1$  Heisenberg model with uniaxial anisotropies on the Shastry-Sutherland lattice – a straightforward generalization of the canonical Shastry-Sutherland model. In addition to the aforementioned theoretical motivation, such a model is potentially relevant to  $\text{RB}_4$  compounds with an integer spin and easy-plane single-ion anisotropy at moderate temperatures – large enough that thermal excitations to the first doublet are finite, but small enough that contributions from the higher doublets are suppressed.

## MODEL

The  $S = 1$  generalization of the Shastry-Sutherland model as studied here is described by the Hamiltonian

$$\begin{aligned} \mathcal{H} = & J \sum_{\langle i,j \rangle} [-\Delta (S_i^x S_j^x + S_i^y S_j^y) + S_i^z S_j^z] \\ & + J' \sum_{\langle\langle i,j \rangle\rangle} [-\Delta (S_i^x S_j^x + S_i^y S_j^y) + S_i^z S_j^z] \\ & + D \sum_i (S_i^z)^2 - B \sum_i S_i^z, \end{aligned} \quad (1)$$

where  $\langle i,j \rangle$  and  $\langle\langle i,j \rangle\rangle$  refer to summation over the nearest neighbors (nn) and along the diagonals of the Shastry-Sutherland lattice (SSL), respectively, and the corresponding interaction strengths are  $J$  and  $J'$  (Fig. 1). Henceforth,  $J$  is set to unity and all the parameters are expressed in units of  $J$ .  $\Delta$  is the measure of the exchange anisotropy - in this work, we consider a strong and constant Ising-like exchange anisotropy,  $\Delta = 0.2$ .

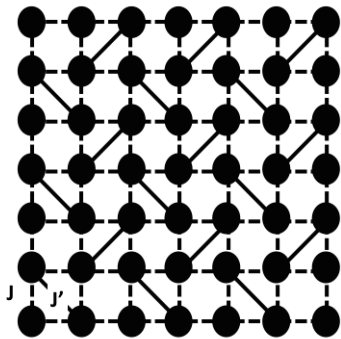


FIG. 1: Shastry-Sutherland lattice. Interaction strengths between nearest neighbors and along alternating diagonals are  $J$  and  $J'$ , respectively.

$D > 0$  measures the magnitude of easy-plane single-ion anisotropy, which is restricted to be easy-plane in this study.  $B$  denotes an external longitudinal magnetic field. The exchange term is chosen to be ferromagnetic - this eliminates frustration in the exchange part of the interaction and as a consequence, the negative sign problem in quantum Monte Carlo (QMC) simulation is alleviated. Frustration is retained in the Ising part of the interaction. In a real quantum magnet, both the exchange and Ising part of the interaction have the same nature, so this may appear unphysical at first sight. But it was shown explicitly for the  $S = 1/2$   $XXZ$  model on the triangular lattice [15, 16] and the generalized  $S = 1/2$  Shastry-Sutherland model [17] (with additional longer range interactions) that in the Ising limit, the ferro- and anti-ferromagnetic exchange interactions can be mapped on to each other. We expect similar arguments to hold for the present model as well.

In the limit of strong easy-axis single-ion anisotropy ( $D < 0$ ), a ferromagnetic exchange appears naturally in the low energy effective model for spin- $S$  systems with integer  $S$  [18]. This low energy effective model turns out to be the  $S = 1/2$  analogue of the model (1), and its ground state phases have been extensively explored [19]. Later, the model was extended by including additional longer range interactions in order to formulate an effective low energy model to capture the magnetic properties of the rare-earth tetraboride family of quantum magnets [13, 14, 17].

The  $S = 1$  model with isotropic antiferromagnetic interaction ( $\Delta = -1$  in the present model) and easy-axis single-ion anisotropy ( $D < 0$ ) was investigated in the framework of coupled chains of orthogonal dimers, using exact diagonalization of small clusters and series expansion methods much earlier in Ref.[20]. In the limit of vanishing single ion anisotropy, the ground state phase diagram is qualitatively similar to that of the canonical  $S = 1/2$  Shastry-Sutherland model: for small values of  $J'$ , the system has long range Néel (AFM) order whereas

for large values of  $J'$ , the ground state is comprised of singlets on the diagonal bonds. However, the plaquette phase that is reported for  $S = 1/2$  at intermediate values of  $J'$ , becomes unstable towards an alternative valence bond solid (VBS) ordering for  $S = 1$  and it is not clear if the plaquette phase is stabilized for any finite range of parameters for the  $S = 1$  Shastry-Sutherland model. A moderate value of  $D$  was found to suppress both VBS phases completely.

For the case of ferromagnetic exchange considered in the present work, the singlet phase at large  $J'$  is replaced by the triplet dimer phase - the ground state is comprised of triplets on the diagonal bonds. At small values of  $J'$ , the ground state has long range Ising like AFM ordering - the  $SU(2)$  symmetry of the Néel state is broken by the Ising-like anisotropy of the exchange term ( $|\Delta| < 1$ ). A superfluid ground state with transverse  $XY$ -ordering is stabilized at intermediate values of  $J'$ .

## METHOD AND OBSERVABLES

We have used the stochastic series expansion (SSE) quantum Monte Carlo (QMC) method with directed loop updates [21] to simulate the Hamiltonian on finite size lattices having dimensions  $L \times L$ , with  $L = 4, \dots, 32$ , in units of the bare lattice spacing. Ground state behavior for finite lattices is accessed by using sufficiently low temperatures - an inverse temperature of  $\beta = 8 \times L$  was found to be sufficient for the range of parameters studied. To characterize the different ground state phases,

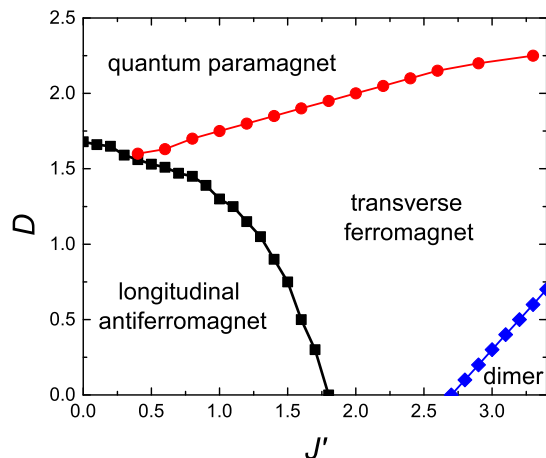


FIG. 2: (Color online) Ground state phase diagram of the  $S = 1$  Shastry-Sutherland model with easy-axis exchange anisotropy and easy-plane single-ion anisotropy. Transitions from longitudinal antiferromagnet to quantum paramagnet and to transverse ferromagnet are of first order while transitions from transverse ferromagnet to quantum paramagnet and to dimer state are continuous.

we have studied the transverse ( $S^{xy}(\mathbf{q})$ ) and longitudinal ( $S^{zz}(\mathbf{q})$ ) components of the static structure factor,

$$\begin{aligned} S^{xy}(\mathbf{q}) &= \frac{1}{N} \sum_{i,j} \langle S_i^x S_j^x + S_i^y S_j^y \rangle e^{i\mathbf{q}\cdot(\mathbf{r}_i - \mathbf{r}_j)}, \\ S^{zz}(\mathbf{q}) &= \frac{1}{N} \sum_{i,j} \langle S_i^z S_j^z \rangle e^{i\mathbf{q}\cdot(\mathbf{r}_i - \mathbf{r}_j)}. \end{aligned} \quad (2)$$

These measure the degree of off-diagonal and diagonal ordering, respectively. Thus, in analogy to supersolids of lattice bosons [22], we can define spin supersolids [23, 24] by the simultaneous presence of transverse and longitudinal order. A useful observable that detects the presence or absence of an excitation gap in any phase is the spin stiffness. A finite stiffness accompanies a gapless state whereas a vanishing stiffness identifies a gapped state. The spin stiffness  $\rho_s$  is defined as the response to a twist in the boundary conditions [25]. In simulations that sample multiple winding number sectors, as in the present implementation of the directed loop algorithm,  $\rho_s$  is simply related to the winding number of the world lines. For square simulation cells in two dimensions,  $\rho_s = (w_x^2 + w_y^2)/2\beta$ , where  $w_x$  and  $w_y$  are the winding numbers in the  $x$  and  $y$  directions [26]. Finally, the uniform magnetization per site  $m = \sum_j \langle S_j^z \rangle / N$  completes the list of observables. In order to probe the ground state properties of the different phases in the thermodynamic limit, we compute the various observables for different system sizes at multiple temperatures and extrapolate the results to the  $T \rightarrow 0$  and  $L \rightarrow \infty$  limits.

## RESULTS

In this section we discuss the multitude of ground state phases that are stabilized for varying ranges of parameters of the model. In accordance with the argument provided earlier, we restrict our investigation to  $\Delta = 0.2$  – a representative value for a strong Ising-like exchange anisotropy. We shall present the results in two parts – first we discuss the ground state phases over different ranges of the single-ion anisotropy ( $D$ ) and the ratio of diagonal to axial nn spin interaction ( $J'$ ) in the absence of an external field. Subsequently, the effects of a longitudinal field and emergent phases are described.

### (i) Ground state phases at $B = 0$

The ground state phase diagram in the  $J' - D$  parameter space, obtained from QMC simulations, is shown in Fig. 2. A value  $\Delta \neq -1$  explicitly breaks the SU(2) symmetry of the model. For small values of  $J'$  and  $D$ , the system exhibits long range longitudinal staggered AFM order – adiabatically connected to the ground state of the  $S = 1$   $XXZ$  model with no single-ion anisotropy

on a square lattice ( $J' = 0, D = 0$ ). The interactions along the diagonals ( $J'$ ) and the single-ion anisotropy ( $D$ ) reduce the magnetic order, but do not suppress it completely at small values. The phase is identified by finite, non-zero values of the longitudinal component of the static structure factor at the AFM ordering vector  $\mathbf{Q} = (\pi, \pi)$ . The transverse component is suppressed reflecting the absence of SU(2) symmetry. The two sublattices of the underlying square lattice (with the diagonals removed) are populated by spins primarily in  $S_i^z = +1$  and  $S_i^z = -1$  states (up to quantum fluctuations). There is a gap to lowest spin excitations resulting in a vanishing spin stiffness. Turning on the diagonal interaction,  $J'$ , opens up a new phases in the ground state phase diagram. As  $J'$  is increased, keeping  $D$  fixed (and small), the frustrated interaction reduces the magnetic order and eventually destroys it at a critical value via a first order quantum phase transition. The suppression of the longitudinal order is accompanied by the onset of transverse ( $XY$ ) ordering with a non-zero value of the transverse component of the static structure factor. The ferromagnetic exchange develops long range order and the ground state is marked by broken U(1) symmetry. This phase is characterized by ferromagnetic ordering (driven by the exchange interaction) in the transverse plane – the spin analog of the bosonic superfluid (SF) state. Analogous to the emergence of Goldstone modes in bosonic superfluids, the gap to lowest excitations vanishes and is reflected in a finite stiffness. Upon increasing the strength of the diagonal interaction further at small  $D$ , the ground state undergoes a continuous quantum phase transition to a gapped phase comprised of dimers along the diagonal bonds. This is the analog of the spin singlet phase in the canonical Shastry-Sutherland model. The dimers in the present model are not singlets, but  $S = 1$  triplets as a result of the ferromagnetic exchange interaction. However, it should be noted that unlike the singlet phase of the canonical model, a direct product of dimers does not constitute an exact eigenstate of the Hamiltonian, but is an approximation valid to leading order in  $1/J'$  [19].

Next we consider the effect of varying the single-ion anisotropy on the nature of the ground states. For small  $J' (\lesssim 0.4)$ , with increasing  $D$ , there is a discontinuous transition from the AFM state to a quantum paramagnetic (QP) phase at a critical value. In the QP phase, each spin is predominantly in the  $S_i^z = 0$  state, due to the energy cost associated with the  $S_i^z = \pm 1$  states for  $D > 0$ . This phase is distinct from the usual paramagnetic state with random spin orientation and is characterized by a finite value of the  $zz$ -component of the nematic tensor,  $Q^{zz} = \langle (S_i^z)^2 - \frac{2}{3} \rangle$ , that is induced by the single-ion anisotropy term [27]. Long range order is suppressed and there is a gap to lowest magnetic excitations. For  $J' \gtrsim 0.4$ , the gapless SF phase is stabilized over a finite range of  $D$  intervening the AFM and QP phases. While the AFM-SF transition remains discon-

tinuous, the SF-QP transition is a continuous one. Finally in the limit of strong interaction along the diagonal bonds ( $J' \gtrsim 2.6$ ), the dimer ground state at low  $D$  gives way first to the SF phase and eventually to the QP phase via two continuous transitions. For intermediate values of  $J'$  ( $1.8 \lesssim J' \lesssim 2.6$ ), the SF phase extends all the way to  $D = 0$ . We notice that, at  $D = 0$ , the phase diagram resembles that of the  $S = 1/2$  model [19].

The transition between the Ising-AFM phase and the quantum paramagnetic phase – both of which have a gap to lowest excitations – is a discontinuous one. On the other hand, the dimer-SF and QP-SF transitions are driven by the breaking of  $U(1)$  symmetry in the SF phase. Hence we expect these transitions to be continuous and belong to the  $O(2)$  universality class. This is confirmed by the scaling of the observables at the associated phase boundaries. For example, it is known from hyper-scaling theory that at a continuous phase transition, the spin stiffness for finite size lattices scale as

$$\rho_s(D, L) = L^{2-d-z} f\left(\frac{D - D_c}{D_c} L^{1/\nu}, \beta/L^z\right),$$

where  $z$  is the dynamical exponent which is unity for the  $O(2)$  universality class. As  $T \rightarrow 0$ ,  $\rho_s(D, L)/L^{2-d-z}$  is a universal function of  $\frac{D - D_c}{D_c} L^{1/\nu}$  and the data for different system sizes collapse to a single curve. At the critical point ( $D = D_c$ ), the ground state stiffness ( $T = 0$ ) scales as

$$\rho_s(D_c, L) = L^{2-d-z}.$$

that is,  $\rho_s(D_c, L)/L^{2-d-z}$  is independent of system size and the curves for different  $L$  intersect at a point, providing an accurate estimate of the critical  $D_c$ . Explicitly, the results are shown in Fig. 3 and Fig. 4.

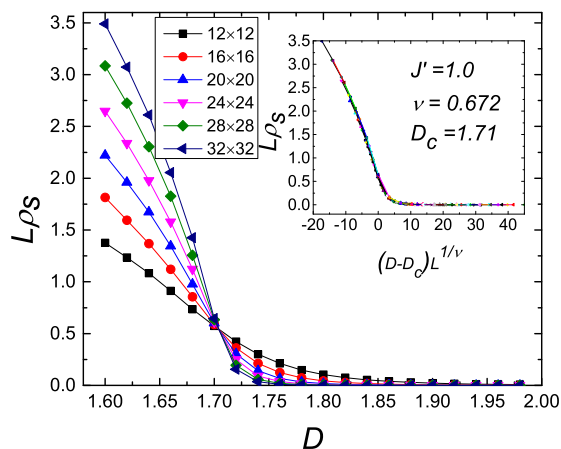


FIG. 3: (Color online) Finite size scaling for the spin stiffness  $\rho_s$  at  $J' = 1.0$ . The critical value  $D_c$  is 1.71(1) and  $\nu = 0.672$ .

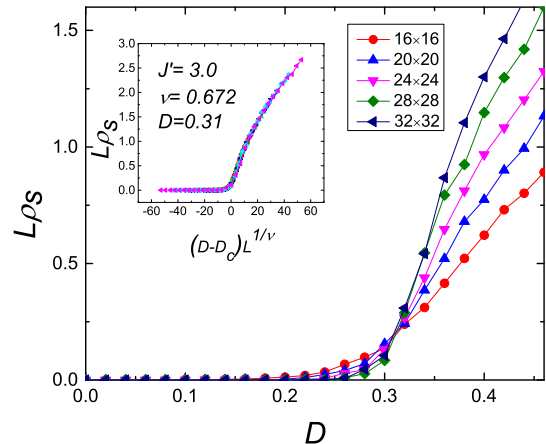


FIG. 4: (Color online) Finite size scaling for the spin stiffness  $\rho_s$  at  $J' = 3.0$ . The critical value  $D_c$  is 0.31(1) and  $\nu = 0.672$ .

## (ii) Ground state phases at $B > 0$

The application of an external longitudinal magnetic field results in the emergence of a wide range of novel ground state phases. The upper panel of Fig. 5 displays the full phase diagram, whose boundaries are obtained by comparing the energies of neighboring phases. In addition to the phases observed at  $B = 0$ , we see multiple magnetization plateaus (PL) with vanishing magnetic susceptibility, and spin supersolid (SS) phases where long range transverse magnetic order coexists with longitudinal magnetic order[28]. For small  $J'$ , the sequence of field-induced phases is qualitatively similar to those obtained for the  $XXZ$  model on a square lattice, viz. longitudinal AFM order with  $\mathbf{Q} = (\pi, \pi)$  ordering - the two sublattices are populated by spins in (predominantly)  $S_i^z = +1$  and  $S_i^z = -1$  states (modulo quantum fluctuations)[23]. The AFM state remains the ground state at small fields till the gap is closed at a critical field strength, beyond which a finite fraction of the spins are flipped from  $S_i^z = -1$  to  $S_i^z = 0$  state, whereas the  $S_i^z = 1$  sublattice remains unaltered. The ground state acquires additional long range transverse ordering via a continuous transition while still retaining the long range longitudinal AFM ordering. In other words, the ground state is a spin supersolid (SS1 in Fig. 5). With increasing field, there is a transition to a longitudinally ordered state with uniform magnetization  $m = 1/2$  (PL1). The ordering corresponds to replacing *all* the  $S_i^z = -1$  spins on the down-sublattice of the AFM state with  $S_i^z = 0$ . The transverse order is completely suppressed and a gap opens up in the excitation spectrum. The magnetization remains constant over a finite range of field reflecting the spin gap – this manifests itself as a plateau in the  $m - B$  curve. At still higher fields, the longitudinal order even-

tually melts and is replaced by an emergent transverse order. Finally, at very large fields, there is a transition to the fully polarized state.

At larger  $J'$ , more interesting phases emerge due to stronger frustration. As the diagonal interaction increases to  $J' \gtrsim 0.8$ , the SS1 and PL1 phases disappear. A new plateau emerges at  $m = 1/3$  (PL2). For  $J' > 1.5$ , the AFM phase also disappears and the sequence of field-induced phases consists of SF-PL2-SF-FP. Upon further increasing the diagonal coupling to  $J' \gtrsim 2.6$ , two new phases appear – a secondary plateau at  $m = 1/6$  (PL3) and a second kind of supersolid (SS2). Finally in the limit of large  $J' (\gtrsim 3.6)$  the zero-field ground state enters the dimer phase – long range magnetic order in the transverse plane is lost. A  $m = 1/2$  plateau (PL4) appears at

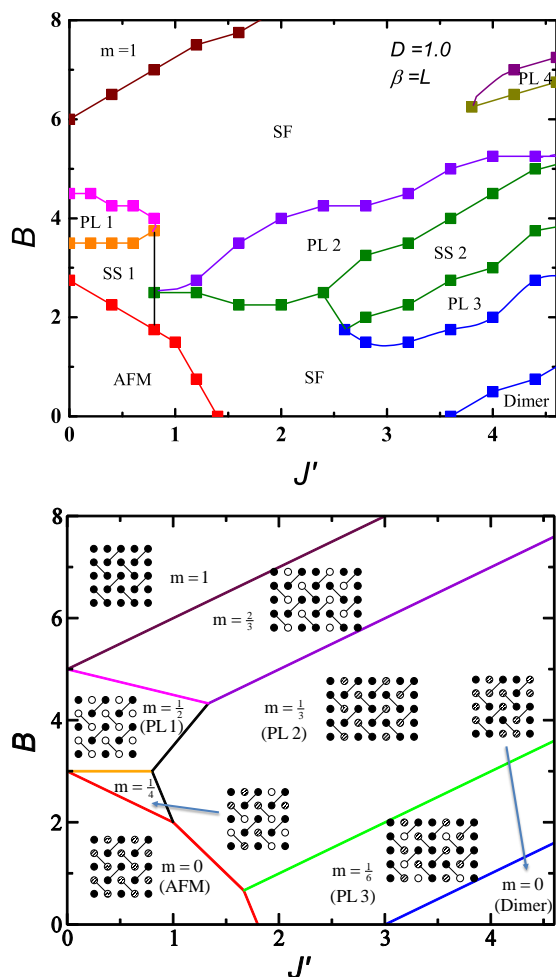


FIG. 5: (Color online) Upper Panel: Full phase diagram of the model at  $\Delta = 0.2$ ,  $D = 1.0$  and  $\beta = L$ . The application of an external longitudinal magnetic field, together with geometric frustration, results in the emergence of a wide range of novel ground state phases, including magnetization plateaus (PL's) and supersolids (SS's). Lower Panel: For comparison, the phase diagram in the Ising limit ( $\Delta = 0$ ) is also shown.

high fields, but the spin structure is markedly different from that in PL1.

In order to better understand the nature of the plateau states, we also compare the energies of possible spin configurations in the Ising limit ( $\Delta = 0$ ) of each plateau and plot the phase diagram along with the local spin structures in Fig. 5. In addition to the plateaus PL1, PL2 and PL3, as well as the zero-field AFM and Dimer phases, in the Ising limit there also exists a  $1/4$  plateau and a  $2/3$  plateau. The  $1/4$  plateau is obtained from the  $1/2$  plateau PL1 by changing the spin states on the  $J'$  bonds from  $(00)$  to  $(\downarrow 0)$ . However, as quantum fluctuations are added to the model, the  $1/4$  plateau becomes unstable towards the formation of the supersolid phase SS1, and by  $\Delta = 0.2$  it has vanished completely. Similarly, the  $2/3$  plateau is unstable towards delocalization of the  $S_i = 0$  spins into a superfluid state. This superfluid state significantly reduces the extent of many of the remaining plateaus. Between the  $1/6$  and  $1/3$  plateaus, the second supersolid phase SS2 emerges. PL4, which does not occur in the Ising limit for  $D = 1$ , emerges at  $\Delta = 0.2$  as a gapped quantum disordered state.

As an illustration of the evolution of the ground state across the multiple phase boundaries, Fig. 6 summarizes the variation of several observables characterizing the different ground state phases as the external field is varied for representative values of the single-ion anisotropy ( $D = 1.0$ ) and diagonal interaction ( $J' = 4.0$ ). The longitudinal magnetization exhibits extended plateaus at  $m = 1/6, 1/3$  and  $1/2$  where the magnetization remains constant over a finite, non-zero field range. As a consequence of its short extent, the plateau at  $m = 1/2$  appears rounded. In the other phases (SF and SS), the magnetization grows monotonically. For the plateaus at  $m = 1/3$  and  $1/6$ , the ground state has long range diagonal order as indicated by the finite value of the longitudinal component of the static structure factor  $S^{zz}(\mathbf{Q})$ , where  $\mathbf{Q} = (2\pi/3, \pi)$  or  $(\pi, 2\pi/3)$  in consideration of symmetry breaking (Fig. 6(b)). In contrast, the nature of the plateau at  $m = 1/2$  (PL4) is quite distinct from the other plateaus (including the other  $m = 1/2$  plateau, PL1) – there is no long range magnetic order as evidenced by the vanishing structure factors (transverse and longitudinal). This state is adiabatically connected to a direct product state of  $\frac{1}{\sqrt{2}}(|\uparrow 0\rangle + |0 \uparrow\rangle)$  along the diagonal  $J'$  bonds. However, like the AFM state (and contrary to the dimer state in the  $S = 1/2$  SSM), the state is not a true eigenstate and the macroscopic degeneracy of the direct product state is lifted by quantum fluctuations. The presence of a finite gap to lowest excitations (and the absence of off-diagonal long range order) is manifested by vanishing values of the spin stiffness,  $\rho_s$ , and the transverse component of the static structure factor,  $S^{xy}(\mathbf{Q})$  for all plateaus (Fig. 6(c)(d)). Conversely, in the range of field strengths  $0.6 \lesssim B \lesssim 2.0$  and  $5.2 \lesssim B \lesssim 6.4$ , the ground state has long range off-diagonal order in the transverse

plane (XY-AFM) marked by finite  $\rho_s$  and  $S^{xy}(\mathbf{Q})$ . Over the intervening range of fields in between the  $m = 1/6$  and  $1/3$  plateaus –  $3.7 \lesssim B \lesssim 4.3$  – the ground state is characterized by simultaneous diagonal and off-diagonal long range order. In other words, the ground state is a spin supersolid.

## DISCUSSION

The emergence of the  $m = 1/6$  plateau and the accompanying spin-supersolid phase are the most interesting results of the present study. These phases arise as a direct consequence of the extended local Hilbert space of  $S = 1$  spins and are absent in the  $S = 1/2$  model. To illustrate this, we show in Fig. 7 the spin arrangements in the  $m = 1/3$  and  $1/6$  plateaus in the Ising limit. Like their  $S = 1/2$  counterpart, the plateaus consist of identical dimers of strongly coupled spins along the diagonal bonds (with  $S^z = 0, 1$ , or  $2$ ) – driven by large  $J'$  – arranged in stripes parallel to one of the principal axes (spontaneously breaking the  $C_4$  symmetry). The magnetization at each plateau determines the modulation of the dimers. The  $1/3$  plateau consists of stripes of  $S^z = +2$  dimers ( $\uparrow\uparrow$ ) and  $S^z = 0$  dimers ( $\uparrow\downarrow$ ) arranged in a regular pattern with periodicity 3 – each period contains two ( $\uparrow\downarrow$ ) stripes and one ( $\uparrow\uparrow$ ) stripe. A

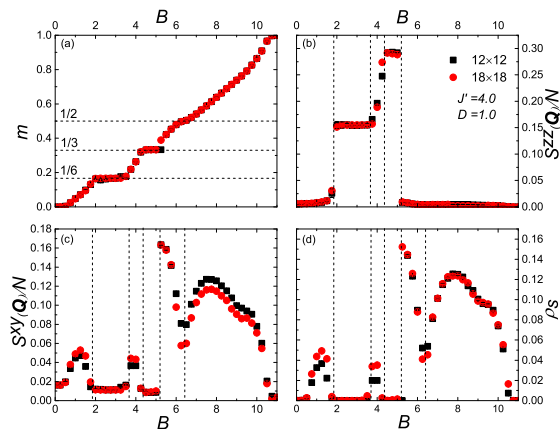


FIG. 6: (Color online) Evolution of the observables with an increasing external field at  $J' = 4.0$  and  $D = 1.0$ . Lattice sizes are  $L = 12$  and  $L = 18$  respectively and reciprocal temperature  $\beta = L$ . (a) Magnetization. The  $1/6$  and  $1/3$  plateaus are prominent; the  $1/2$  plateau is forming. (b) Longitudinal component of the structure factor  $S^{zz}$  at  $\mathbf{Q} = (2\pi/3, \pi)$  or  $(\pi, 2\pi/3)$ . (c) Transverse component of the structure factor  $S^{xy}$  at  $\mathbf{Q}$ . (d) Spin stiffness as a function of magnetic field. Sandwiched between the  $1/6$  and  $1/3$  plateaus ( $3.7 \lesssim B \lesssim 4.3$ ) is a supersolid phase which is characterized by finite  $S^{zz}$ ,  $S^{xy}$  as well as nonvanishing  $\rho_s$ . Error bars are smaller than the symbol size.

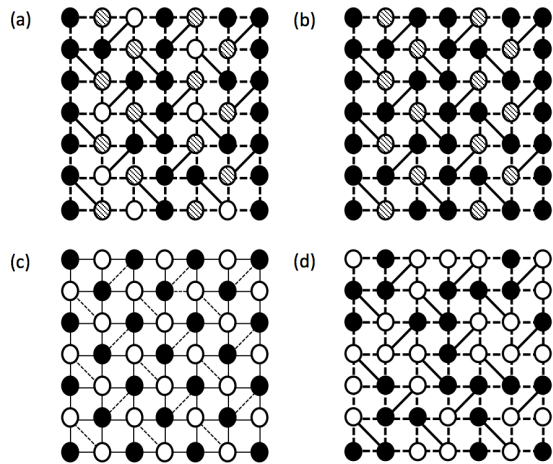


FIG. 7: Schematic structures of the magnetization plateaus. (a)  $1/6$  plateau (PL3 in Fig. 5); (b)  $1/3$  plateau (PL2); (c)  $1/2$  plateau (PL1) with small  $J'$ ; (d)  $1/2$  plateau (PL4) with large  $J'$ . The  $1/6$  plateau and the  $1/3$  plateau are characterized stripe structures. The  $1/6$  plateau is obtained from the  $1/3$  plateau simply by replacing the  $S^z = 2$  ( $\uparrow\uparrow$ ) stripes with  $S^z = 1$  ( $\uparrow 0$ ) stripes. The  $1/2$  plateau in (c) has long range AFM order while the one in (d) is formed by dimers in a superposition of  $S^z = 1$  ( $\uparrow 0$ ) states. Black circles represent  $\uparrow$ ; shaded  $\downarrow$ ; white 0.

peak in the longitudinal structure factor at  $\mathbf{Q}$  confirms this picture. The  $1/6$  plateau is obtained from the  $1/3$  plateau simply by replacing the  $S^z = 2$  ( $\uparrow\uparrow$ ) stripes with  $S^z = 1$  ( $\uparrow 0$ ) stripes, without disturbing the periodicity of the diagonal order – confirmed, once again, by a finite  $S^{zz}(2\pi/3, \pi)$  or  $S^{zz}(\pi, 2\pi/3)$ . The appearance of such “offspring plateau” is a direct consequence of the larger Hilbert space of  $S = 1$  spins and is not realized for  $S = 1/2$  spins. For small values of  $\Delta$ , we anticipate the  $1/2$  plateau to be similarly accompanied by a  $1/4$  plateau, as occurs in the Ising limit. Additionally, it would be interesting to study the competition between the SS2 phase and the putative  $m = 1/4$  plateau, formed as an offspring of the  $1/2$  plateau PL4, in the intervening field range between the  $m = 1/3$  and  $1/6$  plateaus. Unfortunately, our simulations were not suitable to probe the very strong interactions (large  $D$  and  $J'$ ) and anisotropies (small  $\Delta$ ) needed, thus precluding a direct investigation.

The magnetization process going from the  $1/6$  plateau to the  $1/3$  plateau with increasing field involves replacing the ( $\uparrow 0$ ) dimers by ( $\uparrow\uparrow$ ) dimers *continuously*, without altering the ( $\uparrow\downarrow$ ) dimers. At intermediate values of the net magnetization,  $1/6 < m < 1/3$ , a finite number of ( $\uparrow 0$ ) dimers of the  $1/6$  plateau are replaced by ( $\uparrow\uparrow$ ). The stripes with ( $\uparrow\downarrow$ ) dimers remain intact, keeping the diagonal order unchanged. The ground state gains energy by (higher order) delocalization of the extra ( $\uparrow\uparrow$ ) dimers on the sublattice of the ( $\uparrow 0$ ) dimers, thus acquiring off-diagonal long range order. As a result, the

ground state possesses simultaneous diagonal and off-diagonal long range order. In other words, the ground state in this parameter range is a spin supersolid. The underlying mechanism of formation of the spin supersolid phase is similar to that reported earlier for  $S = 1$  spins on a bipartite lattice [23] and bosonic supersolid phase for soft-core bosons with longer range interactions [29].

In conclusion, we have demonstrated the emergence of several new phases in a Spin-1 Shastry-Sutherland model. These include the “off-spring plateaus” described above, as well as two new spin supersolid phases. These new phases appear as a direct result of the enlarged Hilbert space of the  $S = 1$  spins compared to their  $S = 1/2$  counterparts.

We thank Cristian Batista for useful discussions. L.S. acknowledges the support from the CN Yang Scholars Program at Nanyang Technological University. This research used resources of the National Energy Research Scientific Computing Center, which is supported by the Office of Science of the U.S. Department of Energy under Contract No. DE-AC02-05CH11231.

- 
- [1] B. S. Shastry and B. Sutherland, *Physica B+C* **108**, 1069 (1981).
- [2] H. Kageyama, K. Yoshimura, R. Stern, N. Mushnikov, K. Onizuka, M. Kato, K. Kosuge, C. Slichter, T. Goto, and Y. Ueda, *Physical review letters* **82**, 3168 (1999).
- [3] S. Miyahara and K. Ueda, *Physical review letters* **82**, 3701 (1999).
- [4] K. Onizuka, H. Kageyama, Y. Narumi, K. Kindo, Y. Ueda, and T. Goto, *Journal of the Physical Society of Japan* **69**, 1016 (2000).
- [5] H. Kageyama, M. Nishi, N. Aso, K. Onizuka, T. Yoshizawa, K. Nukui, K. Kodama, K. Kakurai, and Y. Ueda, *Physical review letters* **84**, 5876 (2000).
- [6] K. Kodama, M. Takigawa, M. Horvatić, C. Berthier, H. Kageyama, Y. Ueda, S. Miyahara, F. Becca, and F. Mila, *Science* **298**, 395 (2002).
- [7] S. Miyahara and K. Ueda, *J. Phys.: Condens. Matter* **15**, R327 (2003).
- [8] S. Yoshii, T. Yamamoto, M. Hagiwara, A. Shigekawa, S. Michimura, F. Iga, T. Takabatake, and K. Kindo, *J. Phys.: Conf. Ser.* **51**, 59 (2006).
- [9] S. Michimura, A. Shigekawa, F. Iga, M. Sera, T. Takabatake, K. Ohoyama, and Y. Okabe, *Physica B* **378-380**, 596 (2006).
- [10] K. Siemensmeyer, E. Wulf, H.-J. Mikeska, K. Flachbart, S. Gabáni, S. Mat’áš, P. Priputen, A. Efdokimova, and N. Shitsevalova, *Phys. Rev. Lett.* **101**, 177201 (2008).
- [11] M. S. Kim, M. C. Bennett, and M. C. Aronson, *Phys. Rev. B* **77**, 144425 (2008).
- [12] M. S. Kim and M. C. Aronson, *Phys. Rev. Lett.* **110**, 017201 (2013).
- [13] T. Suzuki, Y. Tomita, and N. Kawashima, *Phys. Rev. B* **80**, 180405 (2009).
- [14] T. Suzuki, Y. Tomita, N. Kawashima, and P. Sengupta, *Phys. Rev. B* **82**, 214404 (2010).
- [15] F. Wang, F. Pollmann, and A. Vishwanath, *Phys. Rev. Lett.* **102**, 017203 (2009).
- [16] H. C. Jiang, M. Q. Weng, Z. Y. Weng, D. N. Sheng, and L. Balents, *Phys. Rev. B* **79**, 020409 (2009).
- [17] K. Wierschem and P. Sengupta, *Phys. Rev. Lett.* **110**, 207207 (2013).
- [18] K. Wierschem, Y. Kato, Y. Nishida, C. D. Batista, and P. Sengupta, *Phys. Rev. B* **86**, 201108 (2012).
- [19] Z. Y. Meng and S. Wessel, *Phys. Rev. B* **78**, 224416 (2008).
- [20] A. Koga, N. Kawakami, and M. Sigrist, *J. Phys. Soc. Jpn.* **72**, 938 (2003).
- [21] O. F. Syljuåsen and A. W. Sandvik, *Phys. Rev. E* **66**, 046701 (2002).
- [22] M. Boninsegni and N. V. Prokofev, *Reviews of Modern Physics* **84**, 759 (2012).
- [23] P. Sengupta and C. D. Batista, *Phys. Rev. Lett.* **98**, 227201 (2007).
- [24] P. Sengupta and C. D. Batista, *Phys. Rev. Lett.* **99**, 217205 (2007).
- [25] A. W. Sandvik, *Phys. Rev. B* **56**, 11678 (1997).
- [26] E. L. Pollock and D. M. Ceperley, *Phys. Rev. B* **36**, 8343 (1987).
- [27] Z. Zhang, K. Wierschem, I. Yap, Y. Kato, C. D. Batista, and P. Sengupta, *Phys. Rev. B* **87**, 174405 (2013).
- [28] K.-S. Liu and M. Fisher, *J. Low Temp. Phys.* **10**, 655 (1973).
- [29] P. Sengupta, L. P. Pryadko, F. Alet, M. Troyer, and G. Schmid, *Phys. Rev. Lett.* **94**, 207202 (2005).